



Research

Bio-inspired adsorption sheets from waste material for anionic methyl orange dye removal



A. B. Abdel-Aziz¹ · Khlood A. Alrefaey² · Reem M. El-taweel³ · Husien Sh³ · Kaushik Pal⁴ · Irene S. Fahim² · Lobna A. Said⁵ · Ahmed G. Radwan^{3,6}

Received: 19 May 2023 / Accepted: 13 November 2023

Published online: 27 November 2023

© The Author(s) 2023 [OPEN](#)

Abstract

Nano zero-valent iron (nZVI), bimetallic nano zero-valent iron-copper ($\text{Fe}^0\text{-Cu}$), and Raw algae (*sargassum dentifolium*) activated carbon-supported bimetallic nano zero-valent iron-copper (AC- $\text{Fe}^0\text{-Cu}$) are synthesized and characterized using FT-IR, XRD, and SEM. The maximum removal capacity is demonstrated by bimetallic activated carbon AC- $\text{Fe}^0\text{-Cu}$, which is estimated at 946.5 mg/g capacity at the condition pH=7, 30 min contact time under shaking at 120 rpm at ambient temperature, 200 ppm of M.O, and 1 g/l dose of raw algae- $\text{Fe}^0\text{-Cu}$ adsorbent. The elimination capability of the H_3PO_4 chemical AC- $\text{Fe}^0\text{-Cu}$ adsorbent is 991.96 mg/g under the conditions of pH=3, 120 min contact time under shaking at 120 rpm at room temperature, 200 ppm of M.O, and 2 g/l doses of H_3PO_4 chemical AC- $\text{Fe}^0\text{-Cu}$ adsorbent. The Bagasse activated carbon adsorbent sheet achieves a removal capacity of 71.6 mg/g MO dye solution. Kinetic and isothermal models are used to fit the results of time and concentration experiments. The intra-particle model yields the best fit for bimetallic $\text{Fe}^0\text{-Cu}$, AC- $\text{Fe}^0\text{-Cu}$, H_3PO_4 chemical AC- $\text{Fe}^0\text{-Cu}$ and bagasse activated carbon(CH), with corrected R-Squared values of 0.9656, 0.9926, 0.964, and 0.951 respectively. The isothermal results emphasize the significance of physisorption and chemisorption in concentration outcomes. Response surface methodology (RSM) and artificial neural networks (ANN) are employed to optimize the removal efficiency. RSM models the efficiency and facilitates numerical optimization, while the ANN model is optimized using the moth search algorithm (MSA) for optimal results.

Highlights

1. The $\text{Fe}^0\text{-Cu}$ composite, when combined with activated carbon from Bagasse Pulp (CH), exhibited the most effective decolorization effectiveness for anionic colours present in wastewater.
2. The utilization of composites presents a promising opportunity for efficient dye removal due to its cost-effectiveness and environmentally sustainable nature.
3. The utilization of response surface approach and artificial neural network modelling improves the efficacy of removal processes and treatment techniques.

✉ Irene S. Fahim, isamy@nu.edu.eg | ¹October High Institute for Engineering and Technology, Giza, Egypt. ²Industrial Engineering Program, SESC Research Center, Nile University, Giza, Egypt. ³School of Engineering and Applied Sciences, Nile University, Giza, Egypt. ⁴University Centre for Research and Development (UCRD), Department of Physics, Chandigarh University, Gharuan, Punjab 140413, India. ⁵Nanoelectronics Integrated Systems Center (NISC), Nile University, Giza, Egypt. ⁶Engineering Mathematics and Physics Department, Faculty of Engineering, Cairo University, Giza 12613, Egypt.



SN Applied Sciences

(2023) 5:371

| <https://doi.org/10.1007/s42452-023-05600-8>

SN Applied Sciences
A **SPRINGER NATURE** journal

Keywords Adsorption · Response surface methodology (RSM) · Artificial neural network (ANN) · Moth search algorithm (MSA)

Abbreviation

MO	Methylene orange
ANN	Artificial Neural Network
MSA	Moth Search Algorithm
DLS	Dynamic Light Scattering
FT-IR	Fourier Transform-Infrared
XRD	X-Ray Diffraction
SEM	Scanning Electron Microscope
RA	Raw algae
H3PO4	Chemical activated carbon.
SNNs	Simulated neural networks.
DR	Dubinin–Radushkevich
PFO	The mean free energy
PSO	Pseudo-Second Order
Kf	Freundlich Isotherm Equation Constant (L/mg)
K1	Kinetic rate constant of Pseudo-First-Order Equation (min^{-1})
K2	Kinetic rate constant of Pseudo second-order Equation (min^{-1})

1 Introduction

The issue of water pollution has emerged as a significant global concern, mainly because of industrialization and the discharge of industrial waste into waterways [1]. Among the various sources of water pollution, dye pollution from industries such as textiles, paints, leather, cosmetics, food, paper, and pharmaceuticals are particularly concerning [2]. The textile industry produces 10% of the worldwide dye output, with a staggering 0.8 million tons of diverse hues generated annually [3]. Methyl orange (M.O), a water-soluble anionic azo dye, is commonly used in several industries, including textiles, paints, food processing, and paper manufacturing [4]. According to a survey, the textile, pharmaceutical, leather, and plastic industries annually dispose of 50,000 tons of dyes in the water [5]. Numerous methods have been employed to remove dyes from wastewater, including physicochemical, physical, chemical, adsorption, biological, and electrochemical [5]. Among these methods, adsorption is regarded as one of the most effective wastewater treatment techniques due to its high removal efficiency and straightforwardness [6]. In recent years, magnetic nanosorbents, such as nZVI and bimetallic iron compounds, have been the subject of extensive research for their potential to remove both organic and inorganic contaminants, including chlorinated ethane, hydrocarbons, poly- and monoaromatic hydrocarbons, and polychlorinated biphenyls [7–9]. Various nanotechnologies have been developed to remove pollutants

such as phosphate, nitrate, sulphate, and phosphorus from wastewater [10–12]. Iron-based particles coated with metals such as Ni, and Cu, FeO have been shown to exhibit increased reactivity. CPC, starch, CMC, and guar gum have also been stabilizers for colloidal systems. Bimetallic nanoparticles represent an efficient adsorbent due to their ability to combine the characteristics of two metals and additional ones, resulting in a bimetallic molecule [10]. The size, structure, and morphology of bimetallic nanoparticles significantly affect their performance. The composite material's reducing ability and surface reactivity for eliminating organic molecules and impurities can be enhanced by adding a modest amount of transition metals to nZVI [13]. Furthermore, adsorbents derived from agricultural waste, such as fava beans, raw algae, and bagasse pulp, are highly effective in removing colour from wastewater while generating minimal byproducts. The extraction of sugar from sugarcane bagasse yields sugarcane bagasse pulp, a plentiful waste product resulting from the decline of the paper industry due to the growing popularity of e-books and other forms of online education. Sugarcane bagasse pulp is widely employed in the paper industry due to its cellulose structure, availability, and low cost. Researchers have recently evaluated the adsorption efficiency of citrate-modified sugarcane bagasse pulp for removing methyl orange (MO) under varying conditions, reporting a maximum removal efficiency of 96.42%. These findings suggest that using sugarcane bagasse pulp and its derivatives as an effective adsorbent for MO removal represents a promising avenue for further research [14]. Although raw sugarcane bagasse lacks the mechanical properties required for use as a membrane material, it can still be used for membrane production through various processes such as electrospinning, phase inversion, and dip coating [15]. Used adsorbents can pollute the environment, making disposal difficult. The type of adsorbent material and the impurities absorbed determine the disposal process. The composite sheet employed to remove Methyl Orange (MO) dye can be disposed of safely. The composite sheet is made from agricultural waste, making it sustainable, biodegradable and non-toxic, the composite sheet can be composted or recycled. However, the adsorbent may contain residual contamination and should be treated carefully. Before disposal, the adsorbent can be cleaned with solvents. For environmental compliance, follow local trash disposal requirements. Disposing of spent adsorbents after field application should limit environmental impact and follow appropriate legislation and recommendations [16]. The present study investigated the MO removal performance of sugarcane bagasse pulp and characterized its

structural and surface topography. The adsorption process is influenced by adsorbent concentration, temperature, contact time, pH, starting dye concentration, and particle size. Activated carbon's high specific surface area and porosity of 800 m²/g enhance its adsorption capacity [17]. However, previous optimization studies employed one-factor-at-a-time (OFAT) experiments, and interaction models such as Response Surface Methodology (RSM) and Artificial Neural Network (ANN) combined with optimization algorithms are more efficacious [18]. ANN models can learn linear, nonlinear, and complex variable relationships [19]. In this study, an ANN model was utilized to predict the removal efficiency of MO, and the Moth search algorithm (MSA), a metaheuristic algorithm, was applied to the ANN model to determine the optimal conditions resulting in maximum removal efficiency. Metaheuristic algorithms simulate biological or physical phenomena and can solve optimization problems [20]. The present study explores composite sheets derived from processed agricultural and marine waste for their ability to remove industrial contaminants from aqueous solutions. Langmuir, Freundlich, Sips, Temkin, Fritz-Schlunder, and Redlich-Peterson isotherm adsorption models were employed to understand the adsorption mechanism. In addition, Laguerre pseudo-first order, pseudo-second order, Elovich, and intra-particle diffusion kinetics were examined to understand the adsorption rates and mechanisms. The characterization of the adsorbent bio-composite was carried out using FT-IR and SEM before and after adsorption. A prior study [21] used a polyaniline-based nano-adsorbent to remove Methyl Orange (M.O). The removal efficiency was predicted using RSM, and ANN and DEO were employed to improve the removal efficiency forecasts, outperforming the RSM technique. However, maximal removal efficiency was not assessed in this study. In another study [22], ANN was used to predict the M.O removal effectiveness using polyaniline nano-adsorbent, and OFAT trials were carried out to determine the optimal settings. Additionally, RSM identified the most critical factor affecting removal efficiency. Furthermore, a study was conducted on the Genetic Algorithm (GA) to determine the parameters and orders of three fractional-order chaotic systems [23].

2 Materials

2.1 Collection of adsorbent and adsorbate

The materials utilized in this study include ferric chloride hexahydrate (FeCl₃·6H₂O, 97% purity, LOBA Chemie), copper chloride dihydrate (CuCl₂·2H₂O, BIOCHEM), activated charcoal (LOBA Chemie), ethanol (C₂H₅OH), sodium borohydride (NaBH₄, 95% purity, ADVENT), and (M.O). All

chemicals and reagents employed in this investigation are of high quality. Deionized water was utilized in all experiments. *Sargassum dentifolium* algae were collected from the Red Sea Coast in Ras Ghareb, Egypt.

2.2 Preparation of sugarcane bagasse pulp support

To prepare the composite sheets, starch (20 g) was blended with humid sugarcane bagasse pulp (60 g), followed by the addition of glycerol (47 g) and water (60 g) to the mixture. The components were thoroughly mixed using a magnetic stirrer for 15 min at 150 °C and 200 rpm. Alkyl ketene dimer (AKD) at a concentration of 3% w/w was subsequently added to enhance the strength of the fabricated sheets.

2.3 Preparation of the composite sheets

7 g of activated carbon was mixed with 100 ml of deionized water and subjected to homogenization for 20 min. Subsequently, sheets of bagasse were combined with the activated carbon, and the resulting composite material was utilized in this investigation. The efficacy of the composite sheets in removing Methyl Orange (MO) was evaluated, and preliminary screening tests were conducted to identify the sheet with the highest removal efficiency (RE %) for mixed solutions of MO under uniform conditions of temperature, sheet size, and concentration. Isotherm and kinetic models were employed to gain insights into the adsorption mechanism of the selected composite sheet.

2.4 Preparation of bimetallic (Fe⁰-Cu)/algae activated carbon composites

The collected raw *Sargassum dentifolium* algae were washed, dried, and ground into fine particles. The resulting dried material was then utilized to prepare physical, and chemical activated carbon. For physical activation, the actual weight of the algae was placed in a muffle furnace at 400 °C for 1 h, followed by an increase in temperature to 600 °C for 2 h, and a subsequent reduction in temperature to 300 °C for 15 min [24, 25]. In contrast, chemical activation was performed by adding chemical activators (250 ml of 85% H₃PO₄ or 150 ml of 4 M H₂SO₄ homogeneous mixture) to 50 g of algae and mixing at ambient temperature to create a mixture, which was then carbonized for three hours at 600 °C, rinsed with deionized water until pH = 7 was attained, and dried in an oven at 110 °C [26, 27]. The synthesis of bimetallic Fe⁰-Cu, as illustrated in Eqs. (1, 2), was based on the chemical reduction and coprecipitation technique. Additionally, bimetallic (Fe⁰-Cu)/algae-activated carbon composites (AC-Fe⁰-Cu) were generated in-situ in a single step. In this study, a conical flask

containing 0.1 M $\text{FeCl}_3 \cdot 6\text{H}_2\text{O}$ solution, 0.002 M $\text{CuCl}_2 \cdot 2\text{H}_2\text{O}$ solution, and 1 g/L of the prepared activated carbon (AC) was continuously stirred at 250 rpm. Subsequently, a 0.5 M sodium borohydride (NaBH_4) solution was added dropwise from a burette. The solution was stirred for an additional 20 min after the complete addition of NaBH_4 solution to ensure the completion of the iron ion reduction reaction in the solution. The resulting precipitate was then separated via filtration and washed multiple times with deionized water and ethanol. Finally, the product was dried at 70 °C and stored at room temperature under an ethanol layer [28, 29].

2.5 Material characterization

2.5.1 Fourier transform infrared spectroscopy (FT-IR)

Attenuated Total Reflectance Fourier Transform Infrared (FT-IR) spectroscopy was employed to examine the mid-infrared bands of the samples. A Tensor 27 (Bruker Optics) instrument was utilized for this purpose. Spectra were recorded at room temperature with 128 scans and a resolution of 4 cm^{-1} . The spectra were vector-normalized over the entire wavelength range of 4000–400 cm^{-1} to eliminate any sample thickness or concentration variations. This analytical technique was used to investigate the chemical reactions in the wastewater samples.

2.5.2 Scanning electron microscopy (SEM)

The prepared composite sheets were mounted on a holder using Tissue Tek O.C.T compound and cooled to a solid nitrogen temperature under vacuum. The sheets were then fractured from the side using a platinum-coated blade, and the fractured surface was imaged using a Flex SEM 1000 II scanning electron microscope [30].

2.5.3 Dye removal experiments explanation

A stock solution of M. orange is prepared by dissolving 1g from the powder in 1L dist. H_2O . Serial dilution is designed according to the applied concentration in the different batch experiments. Commercial activated carbon is purchased to be included in the experiments as a comparative study of prepared activated carbon. (M-ETKAL) 721 spectroscopy is applied to the determination of the.

The removal efficiency of the prepared composites was evaluated using 1000 ppm of Methyl Orange (M.O) dye. The concentration of M.O was determined using a UV-Vis spectrophotometer set at a wavelength of 465 nm. The removal efficiency is examined through different pH ranges (3, 5, 7, and 10), contact times from 15 to 180 min, and M.O concentrations from 50 to 500 ppm. The results

of the time and concentration experiments were used to test isotherm and kinetics models. The removal percentages and the removed M.O dye quantity were calculated using Eqs. (1, 2):

$$\text{Sorption [\%]} = [\text{C}_0 - \text{C}_e] / \text{C}_0 * 100 \quad (1)$$

$$\text{qe [mg/g]} = [(\text{C}_0 - \text{C}_e) * \text{V}] / \text{m} \quad (2)$$

In this study, the equilibrium adsorption capacity (q_e , mg/g) and equilibrium concentration of Methyl Orange (C_e , mg/L) were determined using the initial concentration of M.O solution (C_0 , mg/L), volume of M.O dye solution (V , L), and mass of the adsorbent (m , g), according to the following equation: $q_e = (C_0 - C_e) \times V / m$.

3 Results and discussion

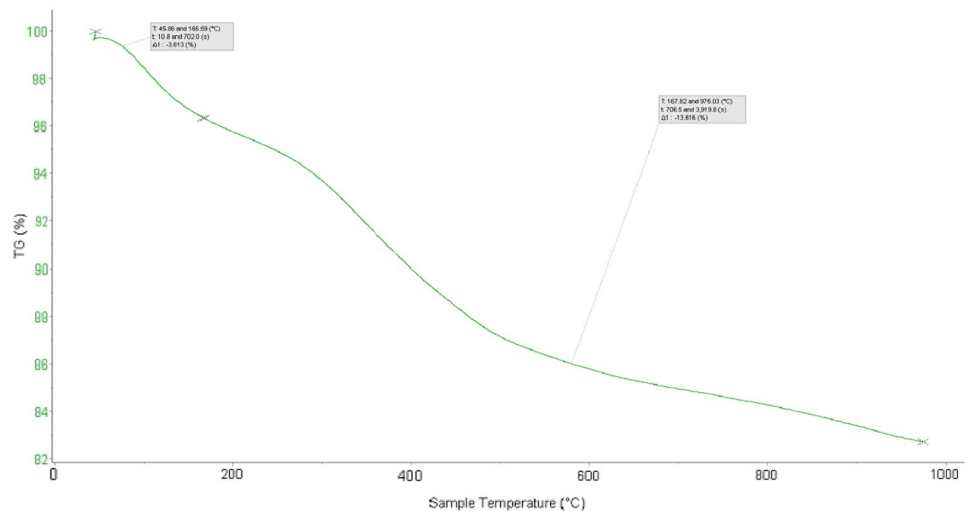
3.1 Characterization of the adsorbent

3.1.1 TGA–DSC for sugarcane bagasse pulp

Figure 1 illustrates the thermogravimetric analysis (TGA) used to investigate bagasse pulp's thermal behavior. The TGA curve showed two distinct regions of weight loss. The first region started at room temperature and ended at around 166.59 °C, which is attributed to the evaporation of surface moisture. The second region, which started at around 167.82 °C and continued up to 975.03 °C, was attributed to the decomposition of the bagasse pulp's cellulose, hemicellulose, and lignin components.

3.1.2 Fourier transform infrared spectroscopy (FT-IR) results for bagasse composite sheet

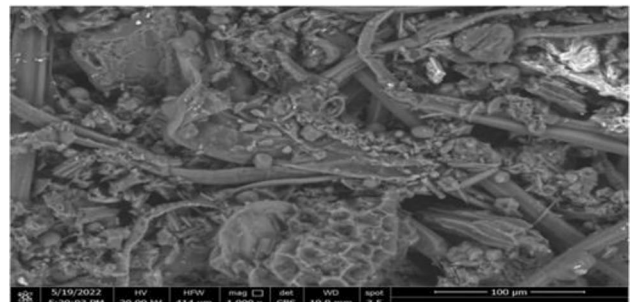
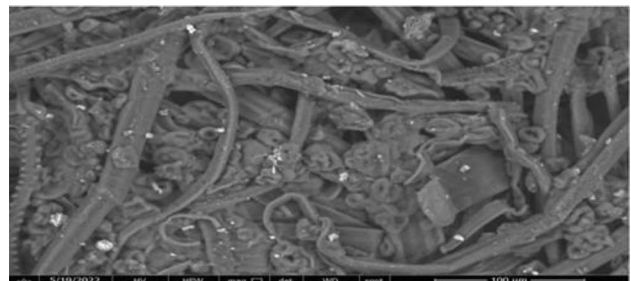
Fourier Transform Infrared spectroscopy is a crucial characterization method to detect the surface functional groups of adsorbent materials. The spectra exhibit similar shapes in the characteristic vibration bands, with high-intensity bands observed between 3200 and 3700 cm^{-1} for O–H and N–H stretching vibrations. The stretching vibrations of aliphatic groups, represented by the symbol CH_2 , are observed at around 2920 cm^{-1} . The bands at approximately 1500 and 1750 cm^{-1} can be attributed to the axial deformation of the C–O molecule, such as highly conjugated C–O stretching or C–O stretching in carboxyl groups. The C–O stretching of carboxylate and ether structures gives rise to bands at roughly 1200 cm^{-1} . These functional groups play a significant role in the absorption of contaminating ions. In the case of natural activated carbon (CH sample), the emergence of peaks at 2890 cm^{-1} and 2827 cm^{-1} resulted in a new peak at 2903 cm^{-1} . Furthermore,

Fig. 1 TGA test for sugarcane bagasse pulp

a new peak at 571 cm^{-1} was observed, while the peak intensity at 1045 cm^{-1} decreased, and the peaks at 1372 cm^{-1} and 1516 cm^{-1} disappeared (Fig. 4). The observed increase in peak intensity indicates a greater abundance of the functional group associated with the molecular bond, while the emergence of new peaks suggests the formation of new bonds resulting from chemical interaction between the pollutants and the sheets via chemical adsorption. These findings indicate that activated carbon possesses numerous functional groups that facilitate the adsorption of contaminant ions.

3.1.3 Scanning electron microscope (SEM) analysis for bagasse sheet

Scanning Electron Microscopy (SEM) is a powerful imaging technique that utilizes a high-energy beam of electrons to observe the surface morphology of materials [31]. Activated carbon is characterized by a porous structure, and the presence of these pores is responsible for its physical adsorption properties. The SEM analysis of the activated carbon coated with sugarcane bagasse pulp composite in the mixed form (Fig. 2) revealed the presence of numerous activated carbon pores. Consequently, physical adsorption occurs on the surface of the composite sheet, leading to the efficient removal of dye particles [11]. Scanning Electron Microscope analysis of the fabricated sugar bagasse pulp sheet is shown in Fig. 3. The surface morphology showed the presence of sugarcane bagasse pulp, starch, glycerol, and AKD. The glycerol particles were easily interpreted in the starch particles which means loss of the free active sites that can contribute to chemical adsorption of the dye's particles. SEM analysis of the surface also showed pores' absence. Therefore, there won't be a place for physical adsorption to take place, and hence this sheet will show low removal efficiency.

**Fig. 2** SEM analysis of sugarcane bagasse pulp sheet coated with activated carbon**Fig. 3** SEM analysis of sugarcane bagasse pulp sheet

Fourier transform infrared (FT-IR) spectroscopy was employed to identify the functional groups present in the synthesized materials. The abundance of functional groups is a crucial factor contributing to the superior adsorption capacity of the adsorbents towards pollutants. Figures 4, 5, raw algae- $\text{Fe}^0\text{-Cu}$ and H_3PO_4 chemical AC- $\text{Fe}^0\text{-Cu}$ exhibited distinct functional groups. Raw algae- $\text{Fe}^0\text{-Cu}$ demonstrated a variety of functional groups, including the OH of carbohydrates at a wavelength of 3421 cm^{-1} , the CH and CH_2 aliphatic stretching at a wavelength of 2923 cm^{-1} ,

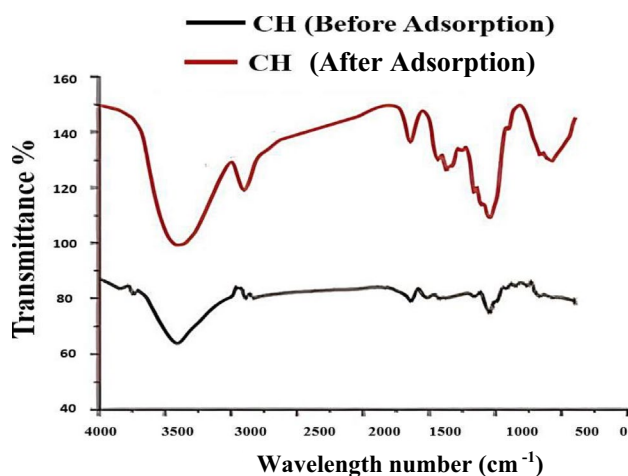


Fig. 4 FT-IR analyses of bagasse composite sheet before and after adsorption. 3.1.4 Fourier transform infrared spectroscopy (FT-IR) of raw algae-Fe⁰-Cu (Bi-RA) and H₃PO₄ chemical AC-Fe⁰-Cu

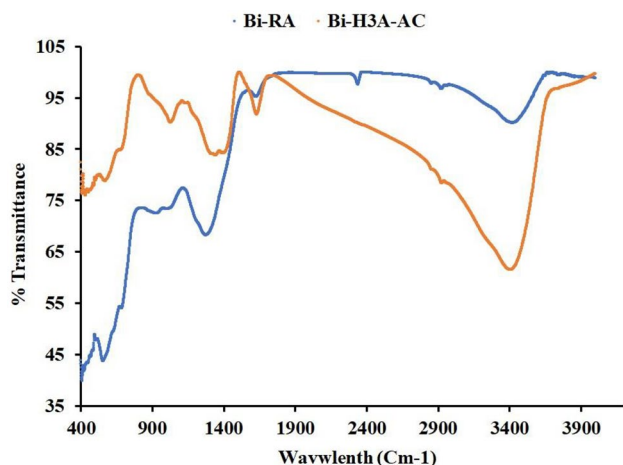


Fig. 5 FT-IR analysis of raw algae-Fe⁰-Cu (Bi-RA) and H₃PO₄ chemical AC-Fe⁰-Cu

and the Amide I of proteins at a wavelength of 1625 cm⁻¹. Additionally, the peak of C-N of amide III was observed at a wavelength of 1273 cm⁻¹, the peak of phosphatidylcholine at a wavelength of 928 cm⁻¹, the peak of C-Cl at a wavelength of 685 cm⁻¹, the peak of C-Br at a wavelength of 555 cm⁻¹, and the peak of alkyl halides at a wavelength of 470 cm⁻¹.

In contrast, the peaks of H₃PO₄ chemical AC-Fe⁰-Cu were observed at OH of carbohydrates at a wavelength of 3419 cm⁻¹, CH and CH₂ aliphatic bending group at a wavelength of 1308 cm⁻¹, C-O-C polysaccharide at a wavelength of 1187 cm⁻¹, and C-O-C polysaccharide at a wavelength of 1138 cm⁻¹. The vibration of CO in the alcohol hydroxyl group was observed at a wavelength of

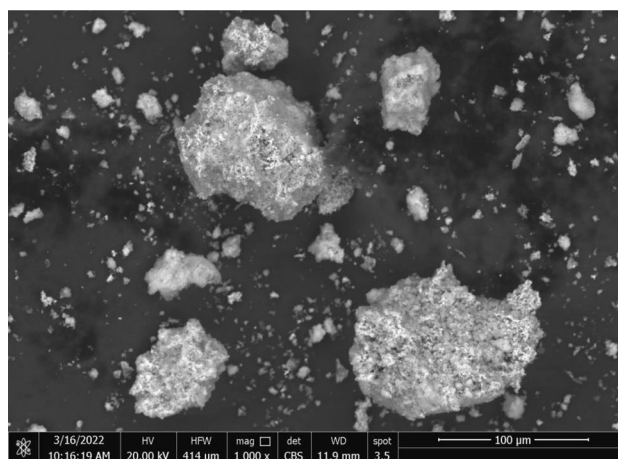


Fig. 6 SEM Analysis of the prepared materials raw algae AC-Fe⁰-Cu (Bi-H₃A-AC)

1025 cm⁻¹, CH bending at a wavelength of 740 cm⁻¹, and CH out of plane aromatic at 708 cm⁻¹. Furthermore, the alkyl halides of C-Cl and C-Br were observed at 676 and 506 cm⁻¹ wavelengths, respectively. These findings provide valuable insights into the molecular characteristics of the synthesized materials and their potential for efficient adsorption of pollutants.

3.1.4 Scanning electron microscopy (SEM) analysis of raw algae bi metallic sheet

Scanning Electron Microscopy (SEM) was employed to examine the surface morphology of the synthesized materials, and the results are presented in Fig. 6. Raw algae AC-Fe⁰-Cu exhibited irregular surfaces with spongy shapes. These results were consistent with the SEM analysis, which indicated aggregation of particles. However, accumulating particles as a sponge increases the surface area and enhances the materials' removal efficiencies towards pollutants. Moreover, the numerous functional groups observed in the FT-IR spectra of these materials suggested that the surface area reduction process was successful. The SEM analysis provided valuable insights into the synthesized materials' surface morphology and particle size distribution, crucial factors affecting their adsorption performance.

3.1.5 Adsorption experiments

3.1.5.1 Isotherm modeling The isotherm models used in the present study were employed to fit the equilibrium data and determine the distribution of the adsorbate between the liquid and solid phases. The models included Langmuir, Freundlich, Sips, Temkin, Fritz-Schlunder, and Redlich-Peterson models. Each model is characterized

Table 1 Parameters of isotherm adsorption models

Isotherm model	Parameters	Values for MO at room temperature
Langmuir	QL	71.63
	KL	16.26
Freundlich	KF	186.4
	nF	1.668
Temkin	KT	217.6
	BT	170.5
Fritz–Schlunder	QFs	21.11
	nFS	1
	KFS	65.71
Sips	S	1
	aS	-21.11
	KS	1387
Redlich-Peterson	RP	1
	KRP	1387
	RP	21.11

by several constants that represent the material's surface properties and adsorption capacity. As shown in Fig. 5, the equilibrium data were fitted to each model, and the corresponding parameters were calculated and tabulated in Table 1. The goodness of fit of the models was evaluated based on the R² and adjusted R² values, presented in Table 2. The Temkin model adequately fits the experimental data, indicating that the adsorption mechanism is likely to involve uniform multilayer adsorption.

Four well-established kinetic models were examined to further analyze the kinetics of Methyl Orange (MO) adsorption onto the composite sheet, including the pseudo-first order, pseudo-second order, Elovich equation, and intra-particle diffusion models. The results presented in Table 3 demonstrate that the adsorption of MO

Table 3 Parameters of kinetics different models

Kinetic model	R ²	Parameters	Values for MO at room temperature
Pseudo-first order	0.9514	Kf (min ⁻¹)	0.01255
		qe (mg g ⁻¹)	8.205
Pseudo-second order	0.9367	Ks (g mg ⁻¹ min ⁻¹)	0.00074
		qe (mg g ⁻¹)	12.11
Elovich	0.9505	(mg g ⁻¹ min ⁻¹)	0.2324
		(g min ⁻¹)	0.3675
Intra-particle diffusion	0.8609	Kid (mg g ⁻¹ min ^{-0.5})	0.5505
		I (mg g ⁻¹)	4.341e-08

onto the composite sheet was accurately described by the pseudo-first-order model, which suggests that the adsorption process is likely to be controlled by surface adsorption. Overall, the results suggest that the Temkin model and the pseudo-first-order kinetic model are appropriate for describing the adsorption behavior of MO onto the composite sheet and that the adsorption mechanism likely involves uniform multilayer adsorption and surface adsorption.

3.1.5.2 Kinetics modeling As shown in Fig. 7, the results of the study suggest that the synthesized adsorbents are adequate for the removal of M.O from aqueous solutions, and the investigation of the adsorption performance under varying experimental conditions provides valuable insights into the adsorption mechanism and the optimal conditions for efficient M.O removal.

The observed concentration dependence of the adsorption capacity is consistent with the Langmuir isotherm, which describes the adsorption process absorbent layer coverage of adsorbate molecules on the adsorbent surface. The increase in adsorption capacity with increasing

Table 2 Calculated error functions for isotherm and kinetic models

Model type	Model name	MO			
		SSE	R ²	Adjusted R ²	RMSE
Isotherm	Langmuir	13.0603	0.9653	0.9794	2.0864
	Temkin	24.7323	0.9708	0.9611	2.8712
	Sips	29.385	0.9653	0.9538	3.1297
	Redlich-Peterson	29.385	0.9653	0.9538	3.1297
	Fritz–Schlunder	29.385	0.9653	0.9538	3.1297
	Freundlich	54.942	0.9352	0.9136	4.2795
Kinetic	pseudo-first order	1.6371	0.9514	0.9382	0.6398
	pseudo-second order	1.6980	0.9489	0.9362	0.6515
	Intra-particle diffusion	2.0982	0.9367	0.9208	0.7242
	Elovich	4.6047	0.8609	0.8262	1.0729

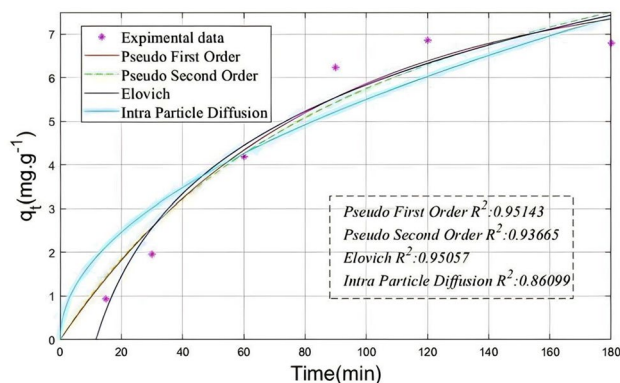


Fig. 7 MO kinetic model fitting

M.O concentration can be attributed to the availability of more adsorption sites on the adsorbent surface as the concentration of M.O in the solution increases.

The observed time dependence of the adsorption process is also consistent with the Langmuir isotherm, which assumes that the adsorption process reaches equilibrium after a certain period. The initial increase in adsorption capacity with increasing contact time can be attributed to the availability of more adsorption sites and the diffusion of M.O molecules from the bulk solution to the surface of the adsorbent. Once equilibrium is reached, a further increase in contact time does not significantly improve the adsorption capacity.

The observed pH dependence of the adsorption capacity can be attributed to the influence of pH on the adsorbent's surface charge and the adsorbate's ionisation. At pH 7, the adsorbent surface is neutral, and the M.O molecules are in their protonated form, allowing maximum electrostatic attraction between the adsorbent and adsorbate. At acidic pH values, the adsorbent surface becomes positively charged, which can repel the positively charged M.O molecules, resulting in decreased adsorption capacity. At fundamental pH values, the adsorbent surface becomes negatively charged, which can repel the negatively charged M.O molecules, also resulting in decreased adsorption capacity.

Overall, the study results are consistent with the Langmuir isotherm and provide valuable insights into the adsorption mechanism and the optimal conditions for efficient M.O removal. The synthesized adsorbents can be optimized for practical applications by controlling the experimental conditions such as concentration, contact time, and pH.

3.1.6 Screening test

A screening test was conducted to evaluate the removal efficiency of the various synthesized materials towards

Methyl Orange (M.O) dye. This test involved subjecting 1 g of the adsorbent material to a 1000 ppm M.O solution with a volume of 1 L, followed by shaking for 3 h. The screening test serves as a preliminary assessment of the adsorption performance of the materials towards M.O dye. It provides a basis for further investigation into the adsorption mechanism and optimal experimental conditions for the efficient removal of M.O dye.

3.1.6.1 Optimization results. Figure 8a depicts removing Methyl Orange (M.O) dye at 15 to 60 g/l concentrations and a three-hour contact time. The findings revealed that the bio-composite mixed sheet containing 60 g had a significantly high removal rate of approximately 87, 92, and 96%. Interestingly, the screening experiments showed that the raw algae AC-Fe⁰-Cu exhibited the highest capacity for M.O dye removal among the various synthesized materials examined. To further explore the optimal adsorption conditions, experiments were conducted with M.O solutions of 500 ppm and a dose of 1 g/l of the adsorbents under constant shaking at 120 rpm at room temperature. The pH values varied between 3, 5, 6, and 8; the results were presented in Fig. 8b. The pH study revealed that the raw algae AC-Fe⁰-Cu had an optimal pH of 3 for M.O dye removal.

Additionally, the adsorption performance was evaluated under varying M.O concentrations ranging from 50 to 500 ppm, and the results are presented in Fig. 8c. The maximum removal efficiency of the raw algae AC-Fe⁰-Cu was 50% at 500 ppm. These findings provide valuable insights into the optimal experimental conditions for efficiently removing M.O dye using synthesized materials. Furthermore, the removal efficiency of M.O dye was evaluated at different contact times spanning 15 to 180 min using 1 g/l of the adsorbents, and the results were plotted against the removal efficiency of M.O and displayed in Fig. 8d. The findings showed that the removal efficiency increased with time and reached a maximum after 120 min, with a removal efficiency of 87.4% for the AC-Fe⁰-Cu sheet.

3.1.6.2 Comparative study on adsorption efficiency of the control group without sheets Treatment A comparative study on the MO dye and without treating with fabricated sheets was evaluated under optimum experimental conditions. It was noticed that using the control group, the estimated values of the final concentration and the dye removal efficiency were 7 mg/L and 70%, respectively. Figures 9, 10, 11 represents the control group of untreated dye under different temperature conditions and PH value.

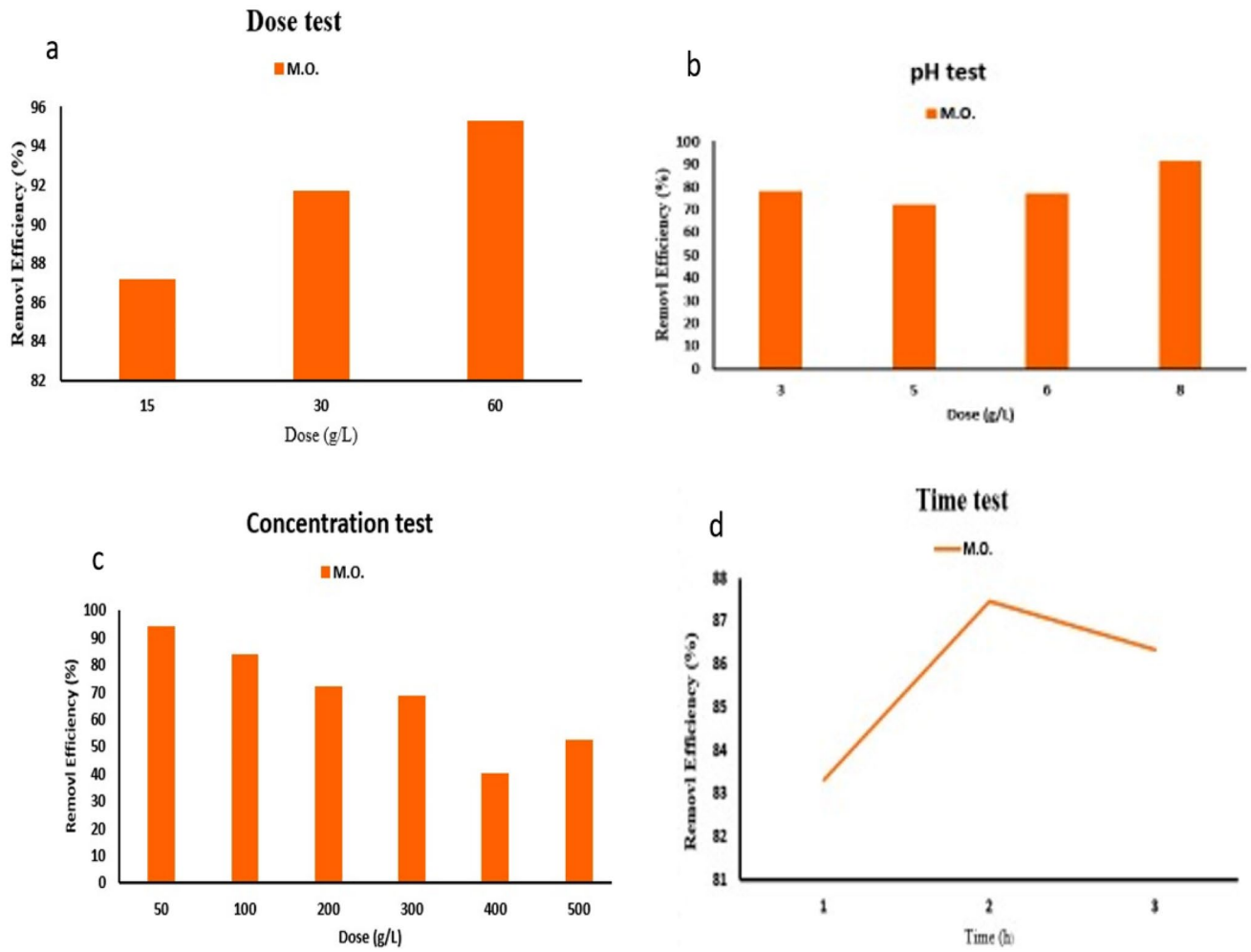


Fig. 8 Optimization parameter results of (a) dose, (b) ph, (c) concentration and (d) Time for the removal efficiency of M.O using raw algae AC-Fe⁰-Cu. sheet

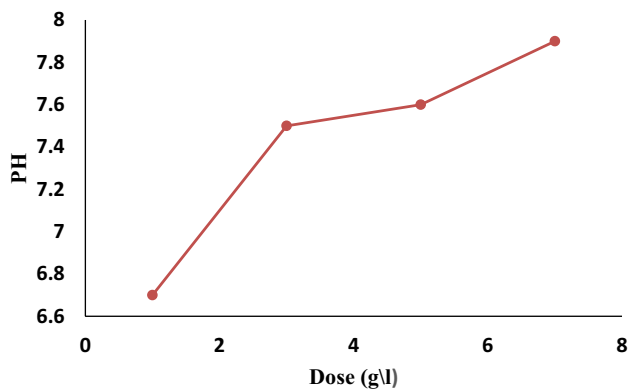


Fig. 9 PH test for untreated dye

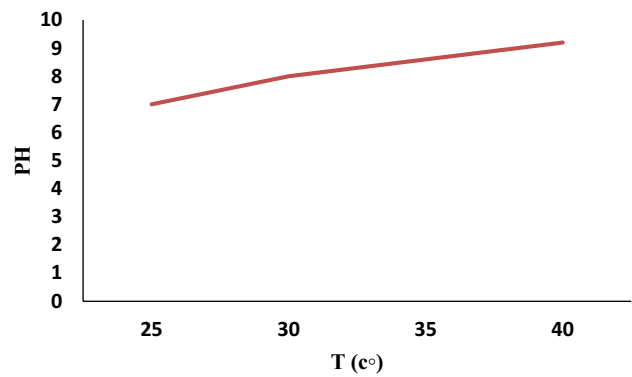
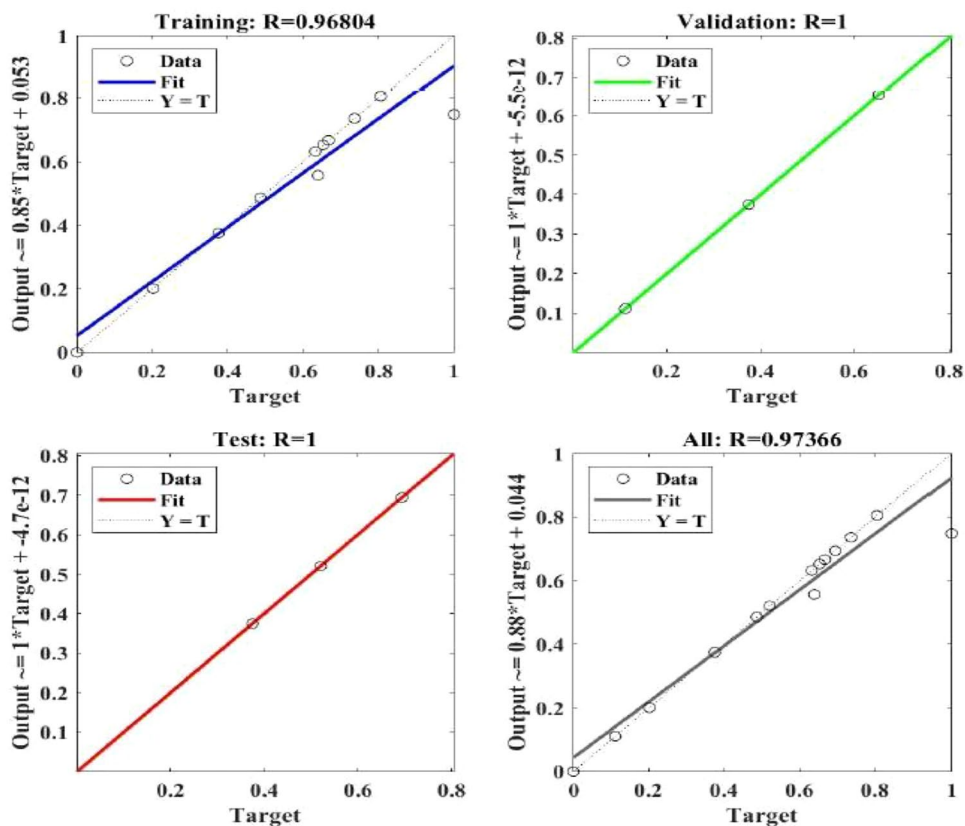


Fig. 10 Temperature test for untreated dye

Fig. 11 The regression plot for the adsorption by raw alga – Fe⁰



3.1.7 Modelling and optimization

Mathematical modelling was employed to establish the relationship between the removal efficiency of pollutants and the three factors, namely concentration, time, and dose. Response Surface Methodology (RSM) and Artificial Neural Network (ANN) models were utilized to predict the removal efficiency under varying conditions of the factors. These models were optimized to identify the maximum removal efficiency and the corresponding factor values. The optimization of the ANN model was performed using the Moth Search Algorithm (MSA). The results obtained from these optimization techniques were experimentally validated. In addition, isotherm and kinetic models were employed to gain insights into the chemical characteristics of the adsorption process. These models provided valuable information on the adsorption type

and the adsorbent’s surface properties. Furthermore, the maximum number of pollutants that can be absorbed was estimated using these models [32]. Using these modelling techniques provides a systematic approach to optimizing adsorption and gaining insights into the underlying chemical mechanisms.

3.1.7.1 Response surface methodology (RSM) Response Surface Methodology (RSM) is a statistical technique utilized to establish a mathematical model that relates the response (dependent variable) to the factors (independent variables). In the present study, the removal efficiency was considered the response, while the concentration, time, and dose were selected as the factors of interest. The low and high levels for each factor were determined, as presented in Table 4. The Face Central Composite Design (FCCD) was chosen as the experimental design, and 20

Table 4 The low and high levels for Concentration, dose, and time

Treat	Levels					
	Concentration (mg/l)		Dose (g/l)		Time (min)	
	Low	High	Low	High	Low	High
H ₃ PO ₄ chemical AC–Fe ⁰ –Cu	100	200	1	2	30	120
Raw alga–Fe ⁰ –Cu	100	200	1	2	30	120

runs with six centre points were conducted. The FCCD was generated using the Design Expert Software, and the laboratory performed the experimental runs. The removal efficiency was evaluated for each run and recorded, and the resulting data were fitted to a quadratic model using the Design Expert Software [33]. The utilization of RSM and FCCD provides a systematic approach to optimizing the experimental conditions and generating a mathematical model to predict the removal efficiency under varying conditions of the factors.

3.1.7.2 RSM for M.O removal by raw algae-Fe⁰-Cu The data in Table 5 fits the quadratic model, as follow:

$$y = 96.22 + 0.0058x_1 + 7.82x_2 - 0.28x_3 - 0.0049x_1x_2 - 0.00029x_1x_3 + 0.016x_2x_3 + 0.000087x^2 - 3.018x^2 + 0.0019x^2 \quad (3)$$

where x_1 , x_2 , x_3 are the removal efficiency, concentration, dose, and time, respectively. The quadratic model is suggested, as shown in Table 6. The quadratic model is selected to fit the data, so the optimum and the interactions between the factors can be evaluated. The quadratic model is not aliased as in the cubic model, and it has $R_2 = 0.7538$.

3.1.7.3 RSM for M.O removal by H₃PO₄ chemical AC-Fe⁰-Cu The data in Table 7 fits the quadratic model, as follow:

$$\text{logit}(y) = 5.489 - 0.006589x_1 - 1.327x_2 - 0.03806x_3 + 0.003575x_1x_2 - 5.324 \times 10^{-6}x_1x_3 + 0.009901x_2x_3 - 2.2458 \times 10^{-7}x^2 - 0.019038x^2 + 0.00019x^2 \quad (4)$$

where y , x_1 , x_2 , x_3 are the removal efficiency, concentration, dose, and time, respectively. The data undergoes a

Logit transformation as a preprocessing step to address nonlinearity and heteroscedasticity issues. Subsequently, a quadratic model is proposed, as indicated in Table 6. This model is deemed suitable for capturing the complexity of the data, enabling the assessment of both the optimum and the interactions between the factors. Notably, the quadratic model is preferred over the cubic model due to its non-aliasing property, which ensures that the model parameters can be uniquely estimated.

3.1.7.4 Artificial neural network (ANN) The data presented in Tables 8 and 9 serve as the input data for the Artificial Neural Network (ANN) implemented using MATLAB R2019a. The ANN architecture comprises an input layer, a hidden layer, and an output layer. Before training the network, the input data is normalized to the range of [0,1], and the number of neurons in the hidden layer is determined based on the minimum Mean Square Error (MSE) criterion. Notably, the ANN model yields superior performance, as evidenced by the higher R-squared (R²) values obtained compared to those obtained using the Response Surface Methodology (RSM), as shown in Figs. 11 and 12. To obtain the optimal parameter settings that maximize the removal efficiency, the ANN is further optimized using the Moth Search Algorithm (MSA), which is a Metaheuristic algorithm that has found successful applications in various domains, such as the optimized edge detection technique for brain tumor detection in MR images [34] and the design and implementation of an optimized artificial human eardrum model [35]. The results of the optimization process denoted as ANN + MSA, are presented in Table 10. Specifically, the optimal combination of raw algae, Fe⁰, and Cu yields a maximum removal efficiency of 92.64%.

Table 5 The fit summary for the adsorption of M.O by raw algae-Fe⁰-Cu

Source	Sequential p value	Lack of Fit p value	Adjusted R ²	Predicted R ²	
Linear	0.9279		-0.1549	-0.6927	
2FI	0.8869		-0.3554	-4.1856	
Quadratic	0.0032		0.5322	-0.7424	Suggested
Cubic	0.0379		0.8245	-67.1120	Aliased

Table 6 The fit summary for the adsorption of M.O by H₃PO₄ chemical AC-Fe⁰-Cu

Source	Sequential p value	Lack of Fit p value	Adjusted R ²	Predicted R ²	
Linear	0.3736	0.3896	0.0173	-0.3482	
2FI	0.4308	0.3690	0.0142	-1.4899	
Quadratic	0.1989	0.4678	0.1787	-1.1772	Suggested
Cubic	0.3041	0.7246	0.3233	-6.3660	Aliased

Table 7 Comparison between nonlinear kinetic models for adsorption using raw algae Fe^0 Cu to remove M.O]

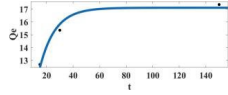
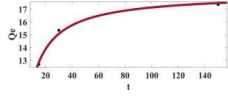
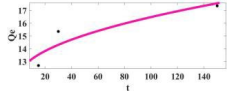
Name	Model	Math. model	Curve fitting	Plot	R^2
Pseudo first order	Nonlinear	$q_t = q_{eq1}(1 - e^{-k_1t})$	$y = 17.9 \cdot 1 - e^{-0.08025x}$		0.9924
Pseudo second order	Nonlinear	$q_t = \frac{K_2 q_{eq2}^2 t}{1 + K_2 q_{eq2} t}$	$y = \frac{19.35x}{x + 7.349}$		0.975
Intra-particle diffusion	Nonlinear	$qt = Kint\sqrt{t} + Cint$	$y = 0.6547\sqrt{x} + 11.15$		0.8114

Table 8 The FCCD for the adsorption of M.O by raw algae Fe^0 Cu, RSM predicted value, RSM residual, ANN predicted value, and ANN residual

Run	Space Type	Concentration	Dose	Time	Removal Efficiency RE %	RSM Predicted RE%	RSM Residual	ANN Predicted RE%	ANN Residual
1	Center	150	1.5	75	91.9214	91.41	0.5152	91.9214	5.24729E-07
2	Factorial	200	1	30	97.7573	96.81	0.9519	95.4074	2.34986822
3	Axial	100	1.5	75	93.2831	91.46	1.83	93.2831	2.9867E-06
4	Factorial	200	2	30	95.9417	95.08	0.8611	95.9417	-3.50625E-05
5	Axial	150	1	75	89.4574	91.03	-1.57	89.4574	-3.25017E-05
6	Factorial	100	2	120	94.5151	95.08	-0.5655	94.5151	1.95004E-05
7	Axial	150	1.5	120	94.5151	95.04	-0.5199	94.5151	1.95004E-05
8	Factorial	200	1	120	95.2932	94.16	1.13	95.2932	3.51931E-05
9	Factorial	100	1	120	94.3854	94.86	-0.4747	93.6201	0.765333552
10	Factorial	200	2	120	94.3206	93.89	0.4266	94.3206	-9.42207E-06
11	Center	150	1.5	75	91.9214	91.41	0.5152	91.9214	5.24729E-07
12	Center	150	1.5	75	91.9214	91.41	0.5152	91.9214	5.24729E-07
13	Axial	150	2	75	90.3003	90.28	0.0248	90.3003	2.61652E-05
14	Factorial	100	2	30	92.9589	93.71	-0.7470	92.9589	-1.1885E-05
15	Axial	200	1.5	75	88.4199	91.79	-3.37	88.4199	-2.0088E-05
16	Center	150	1.5	75	91.9214	91.41	0.5152	91.9214	5.24729E-07
17	Factorial	100	1	30	94.9042	94.94	-0.0402	94.9042	-2.26528E-05
18	Center	150	1.5	75	91.9214	91.41	0.5152	91.9214	5.24729E-07
19	Center	150	1.5	75	91.9214	91.41	0.5152	91.9214	5.24729E-07
20	Axial	150	1.5	30	94.6448	95.67	-1.03	94.6448	5.44964E-06

Table 9 The FCCD for the adsorption of M.O by H₃PO₄ chemical ACFe⁰Cu, RSM predicted value, RSM residual, ANN predicted value, and ANN residual

Run	Space Type	Concentration	Dose	Time	Removal Efficiency (RE)%	Logit (RE)	RSM Predicted Logit (RE)	RSM Residual	ANN Predicted RE %	ANN Residual
1	Factorial	200	2	30	91.2081	2.34	2.45	-0.1146	90.7214	0.486727806
2	Axial	150	2	75	95.0987	2.97	2.48	0.4852	95.1059	-0.007193729
3	Factorial	200	1	30	95.5526	3.07	2.83	0.2414	95.5328	0.019807091
4	Factorial	100	1	30	95.8768	3.15	3.15	-0.0036	94.7713	1.105521963
5	Axial	200	1.5	75	90.6894	2.28	2.45	-0.1761	90.7099	-0.020515989
6	Axial	100	1.5	75	94.7096	2.88	2.62	0.2633	94.7321	-0.022451576
7	Center	150	1.5	75	91.4027	2.36	2.54	-0.1737	91.4121	-0.00944327
8	Center	150	1.5	75	91.4027	2.36	2.54	-0.1737	91.4121	-0.00944327
9	Factorial	200	1	120	94.4503	2.83	2.77	0.0674	94.4571	-0.006823474
10	Factorial	100	2	120	95.4229	3.04	3.30	-0.2632	95.4284	-0.005478858
11	Axial	150	1.5	120	96.2659	3.25	3.13	0.1212	91.9974	4.268479809
12	Factorial	200	2	120	96.3307	3.27	3.29	-0.0182	96.3176	0.013122783
13	Center	150	1.5	75	96.201	3.23	2.54	0.6942	91.4121	4.788936835
14	Factorial	100	1	120	96.201	3.23	3.14	0.0928	96.1968	0.004236835
15	Center	150	1.5	75	91.4027	2.36	2.54	-0.1737	91.4121	-0.00944327
16	Axial	150	1.5	30	93.6073	2.68	2.72	-0.0340	93.5853	0.022017859
17	Factorial	100	2	30	91.1433	2.33	2.42	-0.0892	91.163	-0.019715168
18	Center	150	1.5	75	91.4027	2.36	2.54	-0.1737	91.4121	-0.00944327
19	Center	150	1.5	75	91.4027	2.36	2.54	-0.1737	91.4121	-0.00944327
20	Axial	150	1	75	89.9113	2.19	2.59	-0.3980	89.9437	-0.032431678

3.1.7.5 Kinetic models The Pseudo First Order (PFO), Pseudo Second Order (PSO), and Intra-particle diffusion models were used to curve-fit the data from the laboratory time-dependent studies. For instance, the rate constant (K) values from the Pseudo 1st and 2nd order models can be used to assess M.O. adsorption onto adsorbents and estimate q_e at different contact times. This knowledge can be utilized to design the process and establish the ideal contact time for adsorption. The intra-particle diffusion model shows how rapidly M.O. molecules enter the adsorbent material's holes and how well it operates. By modifying the adsorbent material's particle size, shape, and surface characteristics, this knowledge can increase diffusion and adsorption capacity. A thorough study revealed that PFO and PSO models accurately represent Methyl Orange (M.O) adsorption onto raw algae – Fe⁰–Cu, as shown in Table 7 by superior goodness-of-fit statistics.

The isotherm analysis showed that chemisorption occurs during adsorption, and the PSO model fit the experimental data well. The isotherm study and PSO model fit revealed chemisorption of H₃PO₄ chemical AC-Fe⁰–Cu, as shown in Table 11. Table 12 shows the curve-fitting analysis-estimated kinetic parameters, which reveal the maximal adsorption capacity.

Optimize adsorption with equilibrium isotherm models and thermodynamic parameters using kinetic parameters.

3.1.7.6 Isotherm models The concentration experiments were implemented in the lab, and the data fits Langmuir, Freundlich, Temkin, and Dunbinimm-Radushkevich (D.R.). Temkin and Freundlich are the best fit for the adsorption of M.O. by raw algae – Fe⁰–Cu, as shown in Table 13. The free energy calculated from the D.R. model is higher than 8, as shown in Table 14. Therefore, this adsorption is chemisorption. Temkin and D.R. are the best fit for the adsorption of M.O. by H₃PO₄ chemical AC-Fe⁰–Cu, as shown in Table 15. The free energy calculated from the D.R. model is higher than 8, as shown in Table 16. Therefore, this adsorption is chemisorption.

3.2 Comparison of adsorption capacities and properties of different adsorbents for methyl orange dye removal

The maximum adsorption capacities reported in the literature for different adsorbents, such as activated carbon [36], chitosan/rectorite/carbon nanotubes composite [37], and fly ash modified by Ca (OH)₂/Na₂FeO₄ [38], are 50.8 mg/g, 67.9 mg/g, and 71.63 mg/g, respectively. Using agricultural waste as an alternative adsorbent for MO removal is highly desirable due to the low cost and availability of such materials.

Fig. 12 The regression plot for the adsorption by H_3PO_4 chemical AC- Fe^0

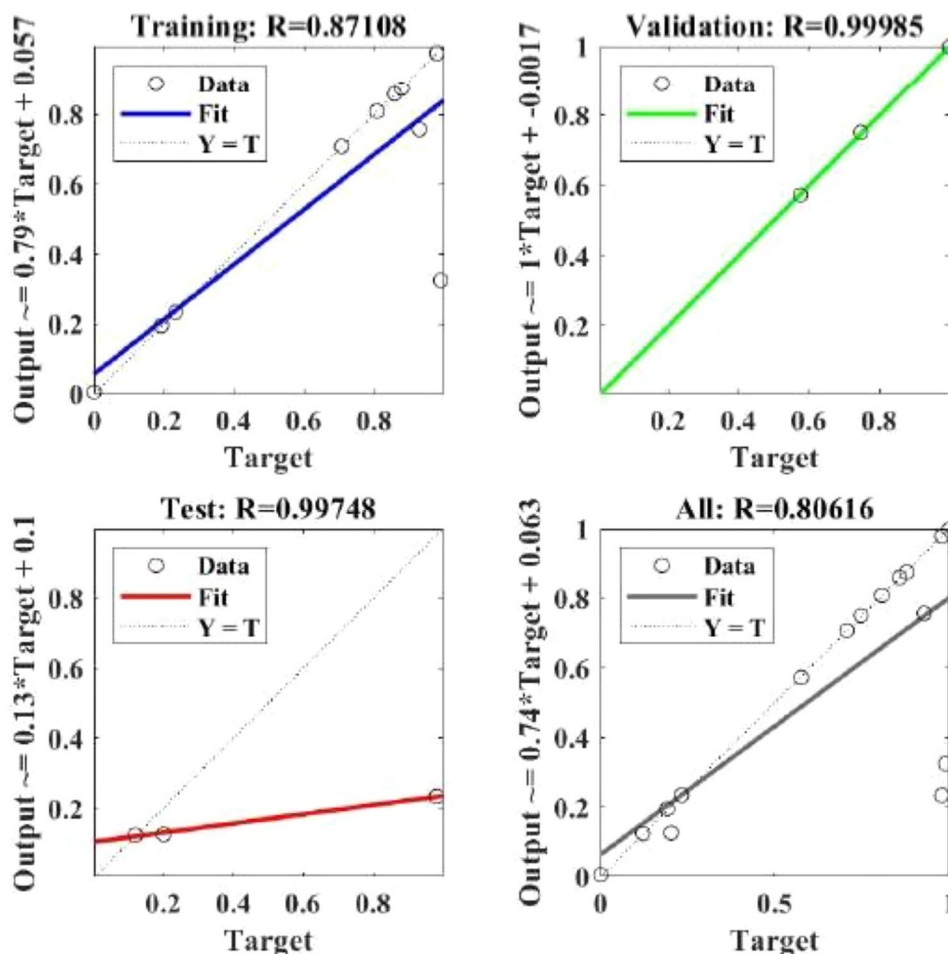


Table 10 The optimization results

Treatment	Concentration	Dose	Time	Predicted RE	Actual RE
H_3PO_4 chemical AC- Fe^0 -Cu	180.7594	1.4656	50.9606	100	85.17781871
raw algae- Fe^0 -Cu	145.4708	1.4111	100	99.8	92.63503748

Activated carbon is a widely used adsorbent due to its high surface area and porosity, providing many active adsorption sites. However, producing activated carbon typically involves high-temperature carbonization, which can result in high energy consumption and greenhouse gas emissions. Chitosan/rectorite/carbon nanotube composite is a promising adsorbent due to its high adsorption capacity and the synergistic effects of the three components [5]. However, the synthesis process is more complex and may be more expensive than other adsorbents. Fly ash modified by $Ca(OH)_2/Na_2FeO_4$ is an effective adsorbent due to the high reactivity of fly ash and the formation of iron oxide species on the surface, which enhance the adsorption capacity. However, using fly ash as an adsorbent may raise concerns about the potential leaching of heavy metals and other

contaminants. Table 14 explains the Advantages and disadvantages of the adsorbents used in methyl orange removal.

The composite sheet used in the present study offers a high adsorption capacity for MO dye and utilizes agricultural waste as a sustainable and low-cost alternative. However, the properties of the composite sheet, such as stability and reusability, need to be further investigated to determine its suitability for large-scale applications.

3.3 Regeneration after adsorption

Regeneration of adsorbents after adsorption is a crucial aspect of the adsorption process, as it can increase the economic and environmental sustainability of the process. Regeneration involves the removal of the adsorbed

Table 11 Comparison between nonlinear kinetic models for adsorption using H₃PO₄ chemical AC–Fe⁰–Cu to remove M.O

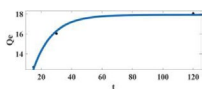
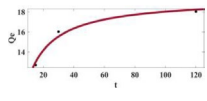
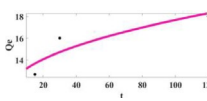
Name	Model	Math. model	Curve fitting	Plot	R ²
Pseudo first order	Nonlinear	$q_t = q_{eq1}(1 - e^{-K_1 t})$	$y = 17.11 \cdot 1 - e^{-0.0864x}$		0.968
Pseudo second order	Nonlinear	$q_t = \frac{K_2 q_{eq2}^2 t}{1 + K_2 q_{eq2} t}$	$y = \frac{18.2x}{x + 6.233}$		0.9886
Intra-particle diffusion	Nonlinear	$qt = K_{int}\sqrt{t} + C_{int}$	$y = 0.4808\sqrt{x} + 11.67$		0.8304

Table 12 kinetic parameters for different models for adsorption using raw algae–Fe⁰–Cu and H₃PO₄ chemical AC–Fe⁰–Cu to remove M.O

Kinetic models	Parameters	Values	
		raw algae–Fe ⁰ –Cu	H ₃ PO ₄ chemical AC–Fe ⁰ –Cu
Pseudo 1st order	q_e (mg/g)	17.9	17.11
	K_1 (1/min)	0.08025	0.0864
Pseudo 2nd order	q_e (mg/g)	19.35	18.2
	K_1 (1/min)	0.00703	0.00882
Intra-particle diffusion	K_{int} (mg/gmin ^{0.5})	0.6547	0.4808
	C_{int} (mg/g)	11.15	11.67

contaminants from the surface of the adsorbent, which allows the adsorbent to be reused for further adsorption cycles. The efficiency of the regeneration process depends on various factors, such as the type and concentration of the desorbing agent, contact time, and temperature [36].

The present study used a composite sheet derived from agricultural waste as an adsorbent for removing Methyl Orange (MO) dye from aqueous solutions. The composite sheet’s maximum adsorption capacity was 71.63 mg/g under the given experimental conditions. The composite sheet’s regeneration can be achieved by desorbing the dye molecules from the surface of the adsorbent using a suitable desorbing agent.

The choice of desorbing agent depends on the nature of the adsorbed molecules and the properties of the adsorbent material. Ethanol, methanol, and acetic acid are commonly used desorbing agents. The desorption efficiency of the composite sheet can be evaluated by measuring the amount of dye molecules desorbed from the surface of the adsorbent. The regenerated adsorbent can then be reused for further adsorption cycles, reducing the need for additional adsorbent material, and increasing the economic sustainability of the adsorption process.

However, it is essential to note that the regeneration process can also have negative environmental

Table 13 Isothermal models comparison for raw alga-*Fe⁰*-Cu adsorption of M.O

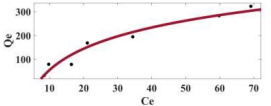
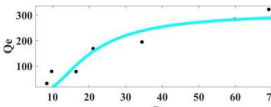
Type	Name	Adsorbent surface	Math. model	Curve fitting	Plot	R ²
Chemisorption	Temkin	The binding energy is uniformly	$q_{eq} = \frac{RT}{b_T} \ln(K_T C_e)$	$y = 128.8 \ln(0.1537x)$		0.9526
			Freundlich	Heterogenous	$q_{eq} = K_F C_e^{1/n_F}$	$y = 11.83 x^{0.782}$
Physisorption	Dubinin-Heterogenous	Heterogenous	$q_e = q_m e^{-\text{Kad} [\text{Rln}(1 + \frac{1}{C_e})]}$	$y = 308.5 e^{-313.3 \ln^2 1 + \frac{1}{x}}$		0.8818

Table 14 Advantages and disadvantages of the adsorbents used in methyl orange removal

Adsorbents	Advantages	Disadvantages
Activated carbon	High surface area and porosity provide many active sites for adsorption	Production typically involves high-temperature carbonization, which can result in high energy consumption and greenhouse gas emissions
Chitosan/rectorite/carbon nanotubes composite	High adsorption capacity and synergistic effects of the three components	Synthesis process is more complex and may be more expensive than other adsorbents
Fly ash modified by Ca(OH) ₂ /Na ₂ FeO ₄	Effective adsorbent due to high reactivity of fly ash and formation of iron oxide species on the surface	Use of fly ash as an adsorbent may raise concerns about potential leaching of heavy metals and other contaminants
Composite sheet from agricultural waste	High adsorption capacity, low-cost and sustainable alternative due to utilization of agricultural waste	Properties such as stability and reusability need to be further investigated for large-scale applications

implications, as the desorbing agent and the desorbed contaminants may need to be disposed of appropriately. The choice of desorbing agent should be made based on its environmental impact and compatibility with local waste disposal regulations. Additionally, the efficiency of the regeneration process should be evaluated against the potential environmental impact of the desorbing agent.

In the regeneration experiment, the spent H₃PO₄ activated carbon sample, which has been used for adsorption, is collected, ensuring proper storage and labelling. A desorption solution is prepared by dissolving 1g of MO powder in 1 liter of water, resulting in a concentration of 1g per liter of MO solution. The MO powder is carefully dissolved in the water to ensure complete dissolution. Subsequently, 1g of the spent H₂PO₄ activated carbon

Table 15 Isothermal models comparison for H_3PO_4 chemical algae $ACFe^0Cu$ adsorption of Methyl orange

Typ	Name	Math. model	Curve fitting	Plot	R^2
Chemisorption	Langmuir	$q_{eq} = \frac{Q_L K_L C_e}{1 + K_L C_e}$	$y = \frac{259.8x}{x+229.7}$		0.908
	Temkin	The binding energy $q_{eq} = \frac{RT}{B_T} \ln(K_T C_e)$	$y = 58.52 \ln(0.04204x)$		0.965
Physisorption	Freundlich	Heterogeno $q_{eq} = K_F C_e^{1/n_F}$	$y = 2.989 x^{0.6929}$		0.869
	Dubinin-Radushkevich	Heterogeneous $q_e = q_m e^{-k_{ad}[R \ln(1 + \frac{1}{C_e})]^2}$	$y = 132.8 e^{-2457[1n(1+\frac{1}{x})]^2}$		0.989

Table 16 Isothermal adsorption parameters for raw algae- Fe^0 -Cu and H_3PO_4 chemical AC- Fe^0 -Cu adsorption of M.O.

Isotherm Models	Parameters	Values	
		raw algae- Fe^0 -Cu	H_3PO_4 chemical AC- Fe^0 -Cu
Langmuir	q_{max} (mg/g)	-	259.8
	K_L (L/mg)	-	0.0044
Freundlich	n	1.2788	1.443
	K_F (L/g)	11.83	2.989
Dubinin-Radushkevich	q_m (mg/g)	308.5	132.8
	K_{ad} (mol^2/kJ^2)	5.0988×10^{-5}	4.145×10^{-4}
	E(kJ/mol)	99.026	34.731
Temkin	β_T	128.8	58.52
	K_T (L/g)	0.1537	0.04204

is placed in a container or beaker, and the prepared MO solution is added, ensuring full immersion of the activated carbon in the desorption solution. The desorption time is set at 180 min based on the determined optimum

time for desorption in the study. To facilitate the desorption process, the mixture of H_2PO_4 activated carbon and MO solution is stirred or agitated using a magnetic stirrer, mechanical shaker, or manual stirring with a glass rod. The

Table 17 The type of the organic solvents which are used in regeneration process in adsorption technique

Regeneration by organic solvents	Methanol, ethanol, isopropanol, ethylene glycol acetone, formalin, and deionized water
Regeneration by Acids	HCL, H ₂ SO ₄
Regeneration by Redox agents	NA ₂ SO ₃ , NA ₂ S, NA ₂ S ₂ O ₄
Used deionized water as a regenerated material	

mixture is allowed to remain in contact for the specified desorption time of 180 min to enable sufficient MO desorption from the activated carbon. After the desorption period, the H₂PO₄ activated carbon is separated from the MO solution using filtration or centrifugation techniques, ensuring the regenerated activated carbon is separated from the desorbed MO solution. The regenerated activated carbon is then rinsed with distilled water to remove any residual MO solution or contaminants from the desorption process, ensuring the removal of impurities and restoration of the activated carbon's adsorption capacity. Finally, the regenerated H₂PO₄ activated carbon is dried thoroughly to remove any remaining moisture. Drying can be achieved using methods such as an oven, vacuum oven, or other suitable drying techniques, ensuring the activated carbon is completely dry to prevent microbial growth or degradation during storage. The maximum removal efficiency of the prepared material, as estimated by the removal efficiency equation as mentioned in Eq. 4 was found to be 50% after regeneration process with 3 trial each trial takes optimum time 180 min consider the removal efficiency of H₃PO₄ material before regeneration was found to be 85.71% The observed decrease in the measured MO dye concentration can be explained by several factors. Initially, the activated carbon can't effectively absorb a significant amount of MO dye from the solution. However, as the treatment continued, the activated carbon reached its adsorption capacity, and any additional MO dye present in the solution was no longer effectively adsorbed. This saturation of the adsorption sites on the activated carbon surface could explain the subsequent increase in the measured MO dye concentration.

3.4 Cost estimation of adsorbent preparation

This present research work involved the use of methyl orange dye. Bimetallic Fe⁰-Cu/Algae Activated Carbon Composites, raw algae-Fe⁰-Cu, and bagasse-activated carbon. To maximize the efficiency of dye removal, activated carbon was prepared from sugarcane bagasse pulp waste and raw algae. Different parameters were examined, and mathematical models were used to determine the effect of the interaction of variables. Since the adsorbent powder is difficult to regenerate, Adsorptive membranes

Table 18 The Materials needed to prepare the bagasse adsorption sheet

Materials to Prepare bagasse adsorption cylinder	The cost
Glycerol (amount-price)	(40.32 g-\$0.64/kg)
Starch (amount-price)	(15 g-\$0.63/kg)
Alkyl ketene dimer (AKD)(amount-price)	(6.81 g-\$0.44/kg)

Table 19 The Materials needed to prepare the raw algae activated carbon bimetallic Fe⁰-Cu sheet adsorption sheet

Chemicals	The cost
250 ml 85% H ₃ PO ₄	\$8
50 g of algae	\$10
1ml FeCl ₃ .6H ₂ O	\$0.10
0.002 M CuCl ₂ .2H ₂ O	\$6
0.5 M sodium borohydride (NaBH ₄)	\$3

were fabricated from sugarcane bagasse pulp and the prepared activated carbon. Different techniques were used for fabrication. Removal efficiency reached 99.1% and was achieved. The following table illustrates organic solvents used in the regeneration process (Table 17). Organic solvents, acids, and redox agents are expensive materials. After the regeneration process, organic solvents must be recycled to use again. Bagasse is considered a solid waste that has no fixed cost.

Following (Table 18) illustrates the cost of the materials needed to prepare the bagasse adsorption sheet.

Based on the printed prices of the materials available in the laboratory as mentioned in Table 19, an estimate of the cost was made. However, the cost of producing this composite would likely be lower if it were manufactured commercially at a larger scale [37].

4 Conclusion

The present study involved the screening of various adsorbent materials, including Bimetallic Fe⁰-Cu/Algae Activated Carbon Composites, raw algae-Fe⁰-Cu, and bagasse activated carbon, for their efficacy in removing

the anionic Methyl Orange (M.O) dye. The adsorption performance of these materials was evaluated under various experimental conditions, and the most effective adsorbents were further characterized using

(FT-IR) and (SEM). Among the tested materials, H_3PO_4 chemical AC-Fe⁰-Cu and Bagasse Pulp + Commercial Activated Carbon exhibited the highest removal efficiencies for M.O. Notably, H_3PO_4 chemical AC-Fe⁰-Cu showed a remarkable removal capacity of 991.96 mg/g under the conditions of pH = 3, 120 min contact time under shaking at 120 rpm at room temperature, 200 ppm of M.O, and 2 g/l doses of H_3PO_4 chemical AC-Fe⁰-Cu adsorbent. Similarly, raw algae-Fe⁰-Cu demonstrated a high removal capacity of 946.55 mg/g under the conditions of pH = 7, 30 min contact time under shaking at 120 rpm at ambient temperature, 200 ppm of M.O, and 1 g/l dose of raw algae-Fe⁰-Cu adsorbent. The characterization results using FT-IR and SEM techniques provide insights into the surface chemistry and morphology of the most effective adsorbent materials. The findings of this study demonstrate the efficacy of sheet-based adsorption for the removal of Methyl Orange (MO) dyes from industrial wastewater. The adsorption behavior of MO onto the composite sheet was evaluated using isotherm and kinetic tests, and the obtained data were analyzed to identify the optimal models. The goodness-of-fit statistics, including Sum of Squares Error (SSE), Root Mean Square Error (RMSE), R-squared (R^2), and modified R-squared, were employed to select the best-fit isotherm and kinetic models. The kinetic study revealed that the pseudo-first-order model effectively described the MO adsorption process. The Temkin isotherm model was identified as the best-fit model for the adsorption isotherm of MO onto the composite sheet, indicating a multi-layer adsorption process with a heat release of 170.5 Joules per mol. The maximum adsorption capacity of the composite sheet, as estimated by the Langmuir isotherm model, was found to be 71.63 mg/g. In addition, the pseudo-second-order model was found to be the best-fit model for the adsorption of MO onto H_3PO_4 chemical AC-Fe⁰-Cu and raw algae-Fe⁰-Cu, with high R^2 values of 0.9886 and 0.9924, respectively. The adsorption process was found to involve both chemisorption and physisorption, as indicated by the Dubinin-Radushkevich isotherm model, which yielded R^2 values of 0.9655 and 0.989 for the H_3PO_4 chemical AC-Fe⁰-Cu and raw algae-Fe⁰-Cu systems, respectively. The Temkin and Freundlich isotherm models were identified as the optimal models for H_3PO_4 chemical AC-Fe⁰-Cu, with R^2 values of 0.9526 and 0.9522, respectively, while the raw algae-Fe⁰-Cu system showed similar R^2 values of 0.9526 and 0.9522 for the Temkin and Freundlich isotherm models, respectively.

Acknowledgements This paper is based upon work supported by the Egyptian Academy of Science, Research, and Technology (ASRT), Project ID: Call no. 2/2019/ASRT- Nexus #4607.

Author contributions A.B. Abdel-Aziz, Reem M. El-taweel, and Husien Sh wrote the results and prepared the figures. Khlood A. Alrefaey, Kaushik Pal, Irene S. Fahim, Lobna A. Said and Ahmed G. Radwan were responsible for data curation and analysis.

Funding Open access funding provided by The Science, Technology & Innovation Funding Authority (STDF) in cooperation with The Egyptian Knowledge Bank (EKB).

Data availability The datasets generated during and/or analyzed during the current study are available from the corresponding author on reasonable request.

Declarations

Conflict of interest There is no conflict of interest.

Open Access This article is licensed under a Creative Commons Attribution 4.0 International License, which permits use, sharing, adaptation, distribution and reproduction in any medium or format, as long as you give appropriate credit to the original author(s) and the source, provide a link to the Creative Commons licence, and indicate if changes were made. The images or other third party material in this article are included in the article's Creative Commons licence, unless indicated otherwise in a credit line to the material. If material is not included in the article's Creative Commons licence and your intended use is not permitted by statutory regulation or exceeds the permitted use, you will need to obtain permission directly from the copyright holder. To view a copy of this licence, visit <http://creativecommons.org/licenses/by/4.0/>.

References

1. Borah P, Kumar M, and Devi P (2020) Types of inorganic pollutants: metals/metalloids, acids, and organic forms. In: *Inorganic pollutants in water*. Elsevier, pp 17–31
2. Hanafi MF, Sapawe N (2020) A review on the water problem associated with organic pollutants derived from phenol, methyl orange, and remsl brilliant blue dyes. *Mater Today: Proc* 31:A141–A150
3. Bayomie OS, Kandeel H, Shoeib T, Yang H, Youssef N, El-Sayed MM (2020) Novel approach for effective removal of methylene blue dye from water using fava bean peel waste. *Sci Rep* 10(1):1–10
4. Kishor R, Purchase D, Saratale GD, Ferreira LFR, Hussain CM, Mulla SI, Bharagava RN (2021) Degradation mechanism and toxicity reduction of methyl orange dye by a newly isolated bacterium *Pseudomonas aeruginosa* mz520730. *J Water Process Eng* 43:102300
5. Das L, Das P, Bhowal A, Bhattacharjee C (2020) Synthesis of hybrid hydrogel nano-polymer composite using Graphene oxide, Chitosan and PVA and its application in waste water treatment. *Environ Technol Innov* 18:100664
6. Chowdhury MF, Khandaker S, Sarker F, Islam A, Rahman MT, and M. R. Awwal, (2020) Current treatment technologies and mechanisms for removal of indigo carmine dyes from wastewater: a review. *J Mol Liquids* 318:114061

7. Crini G, Lichtfouse E, Wilson LD, Morin-Crini N (2019) Conventional and non-conventional adsorbents for wastewater treatment. *Environ Chem Lett* 17(1):195–213
8. Mostafa MK, Mahmoud AS, SaryEl-deen RA, and Peters RW (2017) Application of entrapped nano zero valent iron into cellulose acetate membranes for domestic wastewater treatment. *Proceedings of the Environmental Aspects, Applications and Implications of Nanomaterials and Nanotechnology*
9. El-Shafei M, Mahmoud A, Mostafa M, and Peters R (2016) Effects of entrapped nzvi in alginate polymer on btx removal. In *AIChE Annual Meeting*. San Francisco, CA, vol 1318
10. Mahmoud AS, Farag RS, Elshai MM (2020) Reduction of organic matter from municipal wastewater at low cost using green synthesis nano iron extracted from black tea: Artificial intelligence with regression analysis. *Egypt J Pet* 29(1):9–20
11. Philander SG (2008) *Encyclopedia of global warming and climate change*: AE. Sage, vol 1
12. Nandi BK, Goswami A, Purkait MK (2009) Adsorption characteristics of brilliant green dye on kaolin. *J Hazard Mater* 161(1):387–395
13. Harter T (2003) Groundwater quality and groundwater pollution
14. Scaria J, Nidheesh P, Kumar MS (2020) Synthesis and applications of various bimetallic nanomaterials in water and wastewater treatment. *J Environ Manage* 259:110011
15. Mpatani FM, Aryee AA, Kani AN, Wen K, Dovi E, Qu L, Li Z, Han R (2020) Removal of methylene blue from aqueous medium by citrate modified bagasse: kinetic, equilibrium and thermodynamic study. *Bioresour Technol Rep* 11:100463
16. Zeitoun Z, El-Shazly AH, Nosier S, Elmarghany MR, Salem MS, Taha MM (2022) Electrospinning of polyvinylidene fluoride membranes: effect of membrane composition and fabrication conditions. *Egypt J Chem* 65(2):41–50
17. Jung S-H, Kim J-S (2014) Production of biochar by intermediate pyrolysis and activated carbons from oak by three activation methods using CO_2 . *J Anal Appl Pyrol* 107:116–122
18. Nahali L, Miyah Y, Mejba F, Benjelloun M, Assila O, Fahoul Y, Nenov V, Zerrouq F (2022) Assessment of brilliant green and eriochrome black T dyes adsorption onto fava bean peels: kinetics, isotherms and regeneration study. *Desalination* 245:255–269
19. Mitra S, Mukherjee T, Kaparaju P (2021) Prediction of methyl orange removal by iron decorated activated carbon using an artificial neural network. *Environ Technol* 42(21):3288–3303
20. Abdollahzadeh B, Soleimani Gharehchopogh F, Mirjalili S (2021) Artificial gorilla troops optimizer: a new nature-inspired metaheuristic algorithm for global optimization problems. *Int J Intell Syst* 36(10):5887–5958
21. Karri RR, Tanzifi M, Tavakkoli Yarak M, Sahu J (2018) Optimization and modeling of methyl orange adsorption onto polyaniline nano-adsorbent through response surface methodology and differential evolution embedded neural network. *J Environ Manage* 223:517–529
22. Tanzifi M, Hosseini SH, Kiadehi AD, Olazar M, Karimipour K, Rezaie Mehr R, Ali I (2017) Artificial neural network optimization for methyl orange adsorption onto polyaniline nano-adsorbent: kinetic, isotherm and thermodynamic studies. *J Mol Liquids* 244:189–200
23. Bouchelta C, Medjram MS, Bertrand O, Bellat J-P (2008) Preparation and characterization of activated carbon from date stones by physical activation with steam. *J Anal Appl Pyrol* 82(1):70–77
24. Pallarés J, González-Cencerrado A, Arauzo I (2018) Production and characterization of activated carbon from barley straw by physical activation with carbon dioxide and steam. *Biomass Bioenerg* 115:64–73
25. Kushwaha JP, Srivastava VC, Mall ID (2010) Treatment of dairy wastewater by commercial activated carbon and bagasse fly ash: parametric, kinetic and equilibrium modelling, disposal studies. *Biores Technol* 101(10):3474–3483
26. Charoensook K, Huang C-L, Tai H-C, Lanjapalli VVK, Chiang L-M, Hosseini S, Lin Y-T, Li Y-Y (2021) Preparation of porous nitrogen-doped activated carbon derived from rice straw for high-performance supercapacitor application. *J Taiwan Inst Chem Eng* 120:246–256
27. Hamdy A, Mostafa MK, Nasr M (2018) Zero-valent iron nanoparticles for methylene blue removal from aqueous solutions and textile wastewater treatment, with cost estimation. *Water Sci Technol* 78(2):367–378
28. Eljamal O, Thompson IP, Maamoun I, Shubair T, Eljamal K, Lueangwattanapong K, Sugihara Y (2020) Investigating the design parameters for a permeable reactive barrier consisting of nanoscale zero-valent iron and bimetallic iron/copper for phosphate removal. *J Mol Liq* 299:112144
29. Carlson BD, Donovan DT (2008) *Sem. Sport Mark Q* 17:154–162
30. Akhtar K, Khan SA, Khan SB, and Asiri AM (2018) Scanning electron microscopy: principle and applications in nanomaterials characterization. *Handbook of materials characterization*, pp 113–145
31. Rao GB, Prasad MK, Kumar KK, and Murthy CV, Removal of cadmium (ii) from aqueous solutions using marine macro algae as the sorbing biomass: isotherms and spectroscopic characterization
32. Pezoti O, Cazetta AL, Bedin KC, Souza LS, Martins AC, Silva TL, Júnior OOS, Visentainer JV, Almeida VC (2016) NaOH-activated carbon of high surface area produced from guava seeds as a high-efficiency adsorbent for amoxicillin removal: kinetic, isotherm and thermodynamic studies. *Chem Eng J* 288:778–788
33. El-Naggar NE-A, El-Ewasy SM (2017) Bioproduction, characterization, anticancer and antioxidant activities of extracellular melanin pigment produced by newly isolated microbial cell factories *Streptomyces glaucescens* sp. nov. *Sci Rep* 7(1):42129
34. Abdel-Gawad AH, Said LA, Radwan AG (2020) Optimized edge detection technique for brain tumor detection in MR images. *IEEE Access* 8:243–136
35. Martini BK, Daniel TG, Corazza MZ, de Carvalho AE (2018) Methyl orange and tartrazine yellow adsorption on activated carbon prepared from boiler residue: kinetics, isotherms, thermodynamics studies and material characterization. *J Environ Chem Eng* 6(5):6669–6679. <https://doi.org/10.1016/j.jece.2018.10.013>
36. Chen J, Shi X, Zhan Y, Qiu X, Du Y, Deng H (2017) Construction of horizontal stratum landform-like composite foams and their methyl orange adsorption capacity. *Appl Surf Sci* 397:133–143. <https://doi.org/10.1016/j.apsusc.2016.10.211>
37. Gao M, Ma Q, Lin Q, Chang J, Bao W, Ma H (2015) Combined modification of fly ash with $\text{Ca(OH)}_2/\text{Na}_2\text{FeO}_4$ and its adsorption of methyl orange. *Appl Surf Sci* 359:323–330. <https://doi.org/10.1016/j.apsusc.2015.10.135>

Publisher's Note Springer Nature remains neutral with regard to jurisdictional claims in published maps and institutional affiliations.